THE JOURNAL OF BIOLOGICAL CHEMISTRY VOL. 283, NO. 2, pp. 1197–1208, January 11, 2008

PARP1-dependent Kinetics of Recruitment of MRE11 and NBS1 Proteins to Multiple DNA Damage Sites*

Received for publication, August 14, 2007, and in revised form, November 12, 2007 Published, JBC Papers in Press, November 19, 2007, DOI 10.1074/jbc.M706734200

Jean-François Haince[‡1], Darin McDonald[§], Amélie Rodrigue[¶2], Ugo Déry[¶3], Jean-Yves Masson[¶4], Michael J. Hendzel[§5], and Guy G. Poirier[‡6]

From the [‡]Health and Environment Unit, Laval University Hospital Research Center, Centre Hospitalier Universitaire de Québec, Faculty of Medicine, Laval University, Quebec G1V 4G2, Canada, the [§]Department of Oncology, Faculty of Medicine, University of Alberta and Cross Cancer Institute, Alberta T6G 1Z2, Canada and the [¶]Genome Stability Laboratory, Laval University Cancer Research Center, Hôtel-Dieu de Québec, CHUQ, Québec G1R 2J6, Canada

Poly(ADP-ribose) polymerase 1 (PARP1) is a nuclear enzyme that is rapidly activated by DNA strand breaks and signals the presence of DNA lesions by attaching ADP-ribose units to chromatin-associated proteins. The therapeutic applications of PARP inhibitors in potentiating the killing action of ionizing radiation have been well documented and are attracting increasing interest as a cancer treatment. However, the initial kinetics underlying the recognition of multiple DNA lesions by PARP1 and how inhibition of PARP potentiates the activity of DNA-damaging agents are unknown. Here we report the spatiotemporal dynamics of PARP1 recruitment to DNA damage induced by laser microirradiation in single living cells. We provide direct evidence that PARP1 is able to accumulate at a locally induced DNA double strand break. Most importantly, we observed that the rapid accumulation of MRE11 and NBS1 at sites of DNA damage requires PARP1. By determining the kinetics of protein assembly following DNA damage, our study reveals the cooperation between PARP1 and the double strand break sensors MRE11 and NBS1 in the close vicinity of a DNA lesion. This may explain the sensitivity of cancer cells to PARP inhibitors.

Maintenance of genome stability is essential to successfully complete cellular division and avoid severe consequences, such as carcinogenesis and cell death (1). DNA double strand breaks (DSBs)[7] represent the greatest threat to genome integrity due to its high propensity for loss of genetic material following the repair process. Thus, the DNA damage response includes enzyme activities responsible for the detection, signaling, and repair of damaged DNA as well as the regulation of cell cycle checkpoints and apoptosis that collectively maintain genomic stability (1). Current evidence indicates that the MRN complex is the primary DSB sensor that recruits signaling proteins at DSB sites (2) and that it is essential for the initial damage processing that leads to the recruitment and activation of ATM (3, 4).

Concomitantly, chromatin-associated proteins rapidly become poly(ADP-ribosyl)ated in the vicinity of DNA lesions (5). The involvement of poly(ADP-ribosyl)ation in the repair of DNA single strand breaks (SSBs) by base excision repair has long been recognized (6). However, evidence is accumulating that poly(ADP-ribosyl)ation is also involved in the repair of DSBs by either nonhomologous end joining (NHEJ) (7) or homologous recombination (HR) (8, 9). As a result, cells deficient in proteins involved in these DNA repair pathways are exceedingly sensitive to PARP inhibition (9–11). The major mammalian poly(ADP-ribose) polymerase, PARP1, is activated upon binding to DNA double and single strand breaks, where it synthesizes large amounts of negatively charged ADP-ribose polymers (PAR) (5). Only a few other PARPs have been studied, but their characterization will probably reveal additional functions of poly(ADP-ribosyl)ation (6). The rapid metabolism of PAR is important to release PARP1 from DNA strand breaks (12) and allows the assembly of repair proteins at sites of DNA lesions (13). Persistence of PARP1 and other poly(ADP-ribosyl)ated proteins on DNA will otherwise impede the progression of subsequent signaling and repair pathways (8). On the other hand, failure to generate poly(ADP-ribose) in response to DNA damage by either chemical inhibition or the absence of PARP1 enzyme increases the cellular sensitivity to genotoxic stress (11). This suggests that PAR itself is a key DNA damage signaling molecules (13, 14).

The repair of DNA damage induced by ionizing radiation occurs in the context of chromatin, and it is becoming clear that proteins involved in chromatin remodeling play an integral role in DNA repair (15). Despite increasing evidence for the interplay between ATM and PARP1 (13, 14), an important issue still

* This work was supported in part by the Canadian Institutes of Health Research (CIHR). The costs of publication of this article were defrayed in part by the payment of page charges. This article must therefore be hereby marked "*advertisement*" in accordance with 18 U.S.C. Section 1734 solely to indicate this fact.
[1] Supported by a scholarship from the CIHR Strategic Training Program grant in genomics, proteomics, and bioinformatics.
[2] Recipient of a CIHR doctoral scholarship.
[3] Recipient of a Fonds de la Recherche en Santé du Québec scholarship.
[4] A CIHR New Investigator.
[5] Senior scholar of the Alberta Heritage Foundation for Medical Research.
[6] Holder of a Canada Research Chair in Proteomics. To whom correspondence should be addressed: CHUL Rm. RC-9700, 2705, Laurier Blvd., Quebec, Quebec G1V 4G2, Canada. Tel.: 418-654-2267; Fax: 418-654-2159; E-mail: guy.poirier@crchul.ulaval.ca.
[7] The abbreviations used are: DSB, DNA double-strand break; ATM, ataxia telangiectasia-mutated; ChIP, chromatin immunoprecipitation; HR, homologous repair; IP, immunoprecipitation; MRN, Mre11-Nbs1-Rad50 complex; NHEJ, nonhomologous end joining; PAR, poly(ADP-ribose); PARP, poly(ADP-ribose) polymerase; SSB, single strand break; MEF, mouse embryo fibroblast; DAPI, 4′,6-diamidino-2-phenylindole; FRAP, fluorescence recovery after photobleaching; MOPS, 4-morpholinepropanesulfonic acid; GFP, green fluorescent protein.

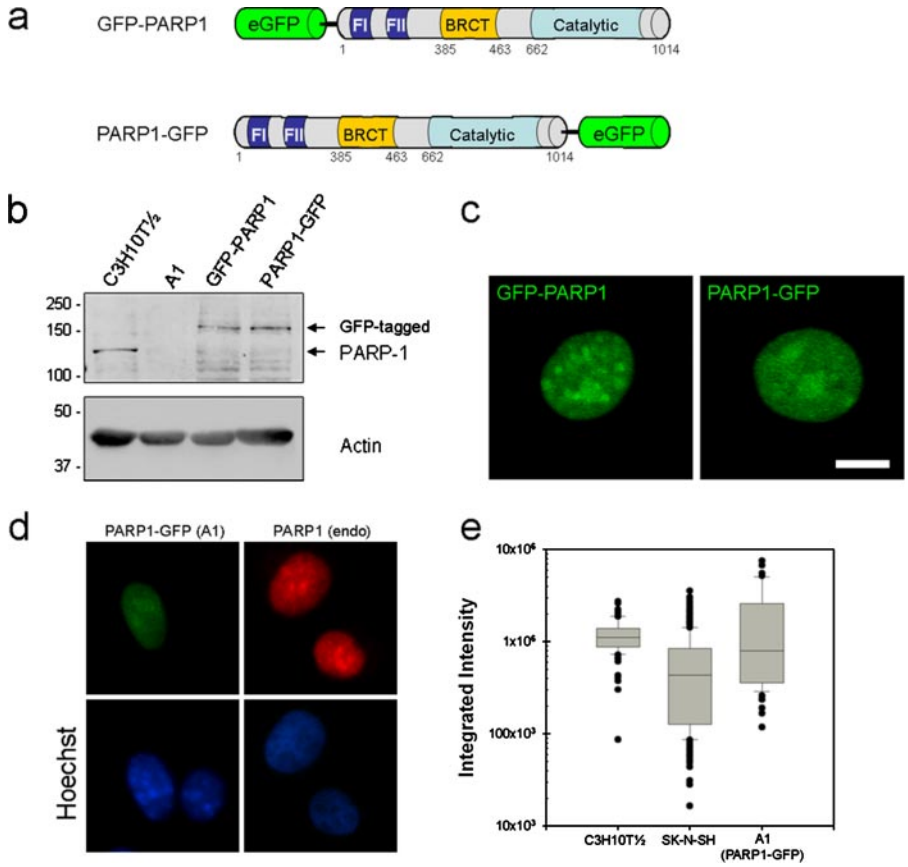

FIGURE 1. **Characterization of GFP-tagged PARP1 expression in PARP1-deficient cells.** *a*, schematic diagram of GFP fusion constructs. The human PARP1 was fused at either its N terminus or C terminus to GFP. *b*, constructions allowing expression of PARP1 fused to GFP were transiently expressed in PARP1-deficient (A1) cells. Total extracts from wild-type (C3H10T$_{1/2}$), PARP1-deficient (A1), and GFP-tagged PARP1-expressing cells were prepared and immunoblotted with anti-PARP1 antibody. Actin blots are shown as a loading control. *c*, GFP image obtained at the onset of the time lapse experiment. *Bar*, 10 μm. *d*, cellular localization was also analyzed by indirect immunofluorescence microscopy using anti-PARP1 monoclonal antibody in order to detect both PARP1-GFP in knock-out cells (A1) (*left*) and endogenous PARP1 in normal cells (C3H10T$_{1/2}$) (*right*). DNA was stained with Hoechst 33342. *e*, for the determination of PARP1 expression in mouse (C3H10T$_{1/2}$), human (SK-N-SH), and PARP1-deficient cells expressing a functional PARP1-GFP construct, multiple fields were examined to count at least 200 cells per cell line. The *graph* presents the integrated fluorescence intensity of nucleus stained with monoclonal antibody (clone C2-10) that recognizes endogenous PARP1. *eGFP*, enhanced GFP.

incompletely resolved is the temporal and spatial relationships among these factors. To address this question in a real time *in vivo* approach, we investigated the early steps of DNA damage signaling involving PARP1 and the MRN complex proteins MRE11 and NBS1 following local microirradiation. In this study, we report the initial kinetics underlying the DNA damage recognition by PARP1 at sites of laser-induced DNA damage using live cell imaging analysis. The analysis shows that PARP1 rapidly accumulates on induced DSBs and that PARP1 promotes the recruitment of MRE11 and NBS1 to these DNA lesions. Moreover, we also provide data showing that MRE11 and PARP1 can interact. The results presented suggest a mechanism by which PAR-binding interaction may contribute to the initial damage signaling that leads to the recruitment of MRE11 to DNA strand breaks.

EXPERIMENTAL PROCEDURES

Expression Plasmid—An expression construct of full-length human PARP1 was obtained by cloning a 3.0-kbp SalI-XbaI polymerase chain reaction fragment, amplified from hPARP1 cDNA (*ATCC* Image Clone 519-3735) with the following primer set: forward (5′-ACGCGTCGACA-TGGCGGAG-TCTTCGGATAA-3′) and reverse (5′-GCTC-TAGAA-TTACCACAGGGAGGTCTTA-3′), in frame to the 5′ end of pEGFP-C1 expression vector (Clontech). Expression of this construct in living cells generates a fluorescently tagged PARP1 (GFP-PARP1). The same strategy was applied to generate a full-length PARP1 with the GFP tag in the C terminus (PARP1-GFP). The expression construct was obtained with the following primer set: forward (5′-CCGCTCGAGGA-TGGCGGAGTCTTCGGATAA-3′) and reverse (5′-CCCCCCGGGCC-TCCAGAACCTGAACCCCACA-GGGAGGTCTTAAA-3′), in frame to the 3′ end of pEGFP-N3 expression vector (Clontech). All constructs sequences were verified by automated DNA sequencing. Cellular localization of fluorescently tagged proteins was assessed in living cells, and expression levels were verified by Western blotting.

Cell Culture—Mouse embryonic fibroblasts (MEFs) derived from PARP1-deficient mice (A1) and human neuroblastoma (SK-N-SH) cells were grown in Dulbecco's modified Eagle's medium supplemented with 10% fetal bovine serum, penicillin (100 units/ml), and streptomycin (100 μg/ml). Normal MEFs (C3H10T½) were maintained in basal Eagle's medium containing 10% fetal bovine serum, 2 mM glutamine, penicillin (100 units/ml), and streptomycin (100 μg/ml). All cell lines were maintained at 37 °C, under a 5% CO_2 controlled atmosphere in a humidified incubator. Transient expression of fluorescently tagged PARP1 was performed in PARP1-deficient MEFs (A1) using Effectene transfection reagent (Qiagen) according to the manufacturer's protocols. YFP-MRE11 and GFP-NBS1 were transiently transfected in both normal (C3H10T½) and PARP1-deficient (A1) cell lines under the same conditions.

Antibodies and Immunofluorescence—PAR synthesis was detected with the rabbit anti-PAR 96-10 antibody. Nuclear foci of DNA damage were visualized using phospho-specific antibodies against ATM S1981 (10H11.E12; Upstate Biotechnology, Inc.) and H2AX S139 monoclonal antibody (JBW301; Upstate Biotechnology). Endogenous mouse and human PARP1 was detected using monoclonal antibody C2-10; MRE11 was detected with monoclonal antibody (clone 12D7;

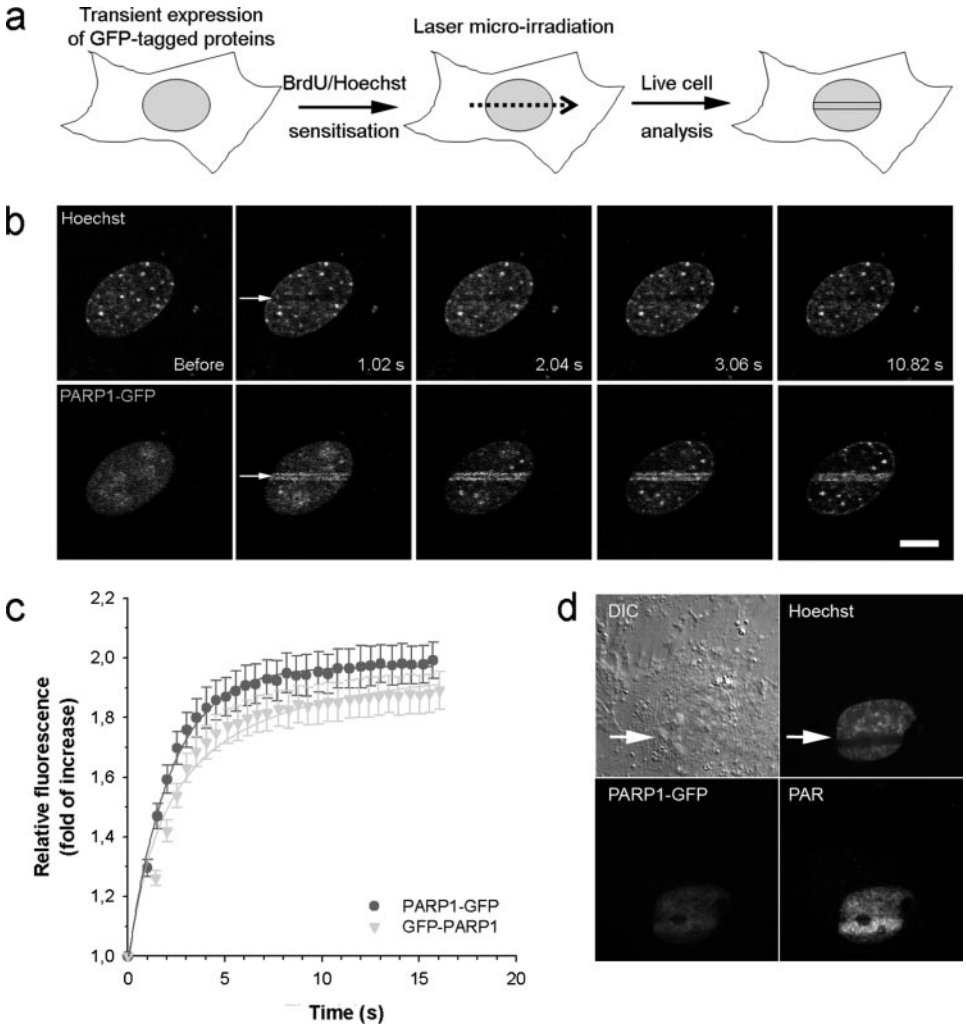

FIGURE 2. **Dynamic assembly of PARP1 at DSB sites.** *a*, scheme of the laser microirradiation experiment. *b*, laser microirradiation induces rapid redistribution of PARP1-GFP at DSB sites. The *top panels* show the photobleaching of Hoechst 33258 dye following microirradiation. PARP1-deficient cells transiently expressing physiological levels of PARP1-GFP (*bottom*) were microirradiated with a 780-nm laser line (10% of maximum laser output) to induce DSBs. The *numbers* at the *bottom right* of each *image* indicate elapsed time (s). *Bar*, 5 μm. *c*, the *graph* shows a plot of intensity *versus* time illustrating the increase in the concentration of both PARP1-GFP and GFP-PARP1 immediately following DSBs induction. Data are presented as mean ± S.E. from at least 10 cells for each construct. *d*, differential interference contrast (*DIC*) images were collected to monitor nuclear membrane integrity and cellular viability 2 min after laser microirradiation. Immunofluorescence shows localization of both PARP1-GFP and PAR polymer after laser microirradiation. The *arrow* indicates the region where DSBs were introduced (1-μm-wide region).

GeneTex). Induction of a single DSB in SK-N-SH cells was performed through transfection of the I-*SceI* expression vector pCBASce using Effectene transfection reagent (Qiagen). For immunofluorescence, cells were fixed immediately after microirradiation (less than 5 min) or at the indicated time points with 4.0% paraformaldehyde in phosphate-buffered saline (pH 7.5) for 15 min at room temperature. Cells were immunostained with combinations of antibody specified in the figure legends. Coverslips were washed twice with phosphate-buffered saline prior to a 30-min incubation with an appropriate secondary antibody conjugated to a fluorophore. Finally, paraformaldehyde-fixed cells were counterstained with DAPI or Hoechst 33258 to stain DNA. Cells were observed using a Zeiss microscope (Axioplan IIM) equipped with a CoolSnapHQ cooled CCD camera. Z-series confocal image sets were collected with a pinhole aperture set to 1.0 Airy units. Images were collected using a 1.3 numerical aperture ×40 PlanFluor objective. The measurement of fluorescence intensity and colocalization was performed using MetaMorph 6.0 (Universal Imaging) software. Composite figures of collected images were assembled in Adobe Photoshop.

Two-photon Microirradiation—We carried out laser microirradiation by modifying a previously described method (16). Cells grown on coverslips were labeled with 1 μM 5′-bromo-2′-deoxyuridine overnight. Cells were placed in fresh medium, exposed to 1 μg/ml Hoechst 33258 for 1 h, and then placed on the stage of a Zeiss LSM510 NLO laser-scanning confocal microscope. DSBs were generated along a 1-μm-wide region across nucleus of a single living cell by excitation of the Hoechst 33258 dye using a near-infrared 780-nm titanium-sapphire laser line. The laser output was set to 10% (unless stated otherwise), and we used 10 iterations to generate localized DSB clearly traceable with a ×40 objective. Protein accumulation within the laser path was compared with an undamaged region within the same microirradiated cell. Therefore, each cell provides a reference unirradiated region that provides high sensitivity to detect and measure small changes in the concentration of fluorescently tagged proteins. For microirradiation, we selected cells with low expression levels and normalized the fluorescence intensity in the microirradiated area to the initial fluorescence in the whole nucleus in order to compensate for photobleaching during acquisition. The average accumulation ± S.E. of fluorescently tagged proteins from at least 10 cells from three independent experiments was plotted.

Fluorescence Recovery after Photobleaching—FRAP experiments were conducted essentially as described (17, 18). FRAP analysis was carried out with living HeLa cells transfected with PARP1-GFP fusion proteins. A laser-scanning confocal microscope (Zeiss LSM 510) equipped with a 488-nm laser light and a 40 × 1.3 numerical aperture objective was used to perform all photobleaching experiments. Fluorescence recovery was monitored over a 40-s period. Data obtained for recovery were corrected for the background intensity and loss of total fluorescence.

Chromatin Fractionation—Normal MEF cells and PARP1-deficient cells were treated or not with etoposide (50 μM). One

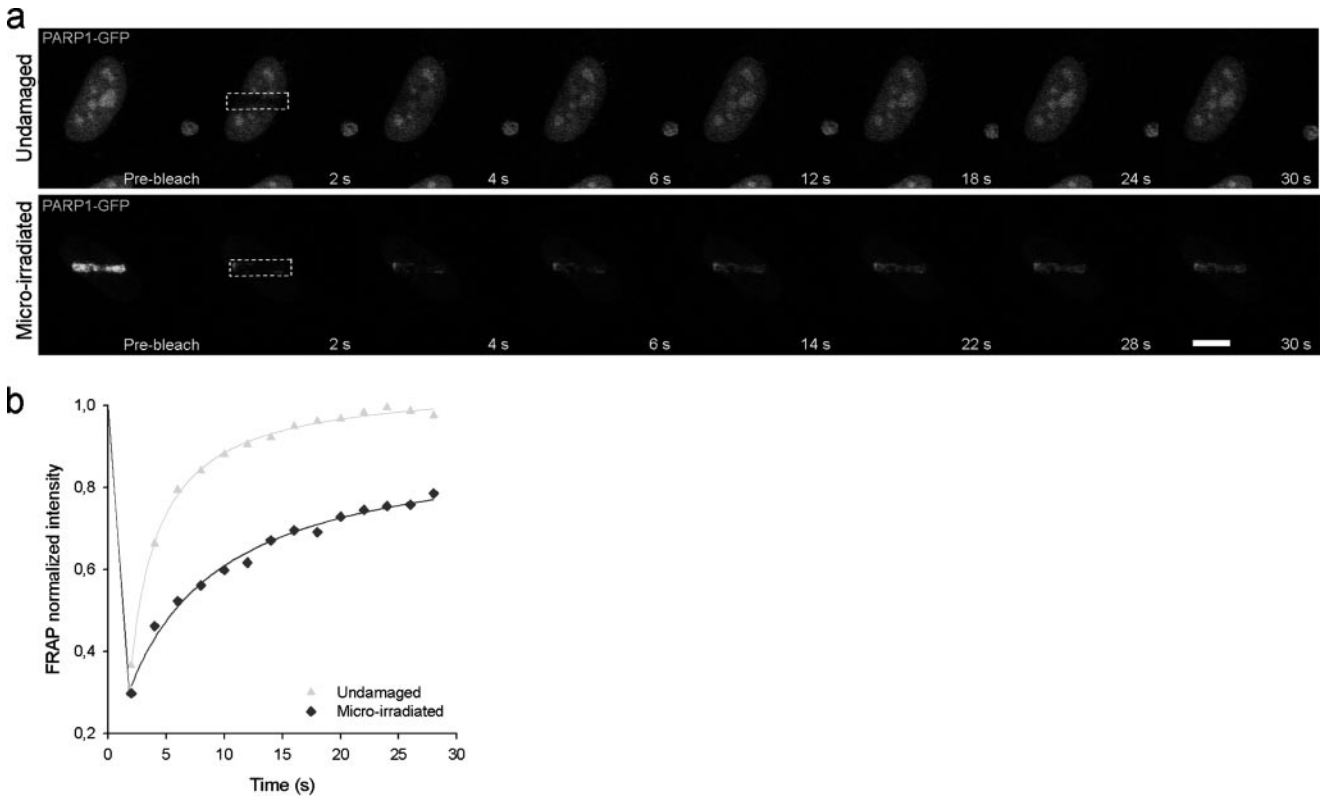

FIGURE 3. **FRAP analyses of PARP1-GFP in undamaged and microirradiated nuclei.** *a*, the *upper panel* shows the time-lapse image collection of PARP1-GFP recovery after photobleaching in undamaged HeLa cells. The *bottom panel* shows FRAP images of PARP1-GFP inside the microirradiated regions. The undamaged nucleoplasm and microirradiated region where FRAP was performed are indicated by a *white box*. *Bar*, 5 μm. *b*, the plot shows normalized mean values of fluorescence intensity *versus* time in seconds after photobleaching.

hour later, cells were biochemically fractionated, and MRE11 retention assays were performed as described (19).

Immunoprecipitation, PAR-binding Assays, and MRE11 Exonuclease Assays—SK-N-SH cells were treated or not with etoposide (50 μM). One hour later, cells were resuspended in lysis buffer (25 mM sodium phosphate buffer, pH 8, 150 mM NaCl, 1 mM EDTA, 0.2% Nonidet P-40, 1 mM dithiothreitol, 1 mM phenylmethylsulfonyl fluoride, and Complete^{TM} protease inhibitors), and endogenous PARP1 and MRE11 were immunoprecipitated essentially as described (13) using the anti-PARP1 monoclonal antibody (clone F1-23) or the anti-human MRE11 monoclonal antibody (clone 12D7; GeneTex). Induction of a single DSB in cells was performed through electroporation of the I-*SceI* expression vector pCBASce, and ChIP was performed with monoclonal antibodies against PARP1 (clone F1-23) as previously described (20). The recombinant MRE11 and MRE11 R/A mutant proteins were produced from baculovirus-infected Sf9 cells, using the Bacto-Bac expression system (Invitrogen) and purified as described (21). PAR-binding affinity was assayed on purified recombinant proteins following separation by SDS-PAGE and transfer onto a nitrocellulose membrane (0.05-μm pore seize). Membranes were incubated with ^{32}P-labeled automodified PARP1 or ^{32}P-labeled purified PAR, washed extensively, and subjected to autoradiography or analyzed by Cerenkov counting using an InstantImager system (PerkinElmer Life Sciences). MRE11 exonuclease assays were conducted in a reaction mixture containing 100 nM DNA in MOPS buffer (25 mM MOPS, pH 7.0, 60 mM KCl, 0.2% Tween 20, 2 mM dithiothreitol, and 5 mM $MnCl_2$) and the indicated amount of PAR. After 5 min at 37 °C, the indicated amount of MRE11 was added, and incubation was continued for 1 h. Reaction products were analyzed by 10% urea-PAGE followed by autoradiography.

RESULTS

Dynamics of PARP1 Recruitment to DNA Damage Lesions—We carried out live cell imaging analysis using MEFs derived from the PARP1 mutant mice and complemented with a functional GFP-tagged PARP1 protein (Fig. 1*a*). Proper expression of the fusion protein was confirmed by Western blotting (Fig. 1*b*). Confocal analyses of transiently transfected cells confirmed the nuclear localization of cells expressing physiological levels of PARP1 tagged with GFP at either its N or C terminus (Fig. 1*c*). Immunofluorescence quantification established that the level of fluorescently tagged PARP1 expressed in PARP1-deficient cells is comparable with levels of endogenous PARP1 in two different wild-type cell lines (Fig. 1, *d* and *e*). To study the recruitment of PARP1 to DNA lesions in living cells, we employed an innovative microirradiation process using near-infrared (780-nm) multiphoton excitation of the Hoechst 33258 dye in living cells that have incorporated 5′-bromo-2′-deoxyuridine into their DNA (Fig. 2*a*) (15, 22). Laser-induced microirradiation produces a variety of DNA lesions, including SSBs, and base damage, but it is best known for its ability to produce DSBs. Moreover, sensitization of cells by 5′-bromo-2′-deoxyuridine incorporation promotes the formation of DSB upon local irradiation (23). This technique allows the introduc-

tion of high levels of DSBs without the toxicity associated with the UV-based laser irradiation approach (15, 16, 23, 24) and offers the advantage of temporal analysis of events and kinetics without requiring intermediate steps, such as fixation, permeabilization of cells, and postfixation staining of proteins.

To monitor the recruitment of PARP1 to DNA lesions, time lapse images have been collected immediately after microirradiation and over a 2-min period. We consistently observed that the recruitment of PARP1 at localized DNA breaks starts less than 1 s after laser microirradiation, and the time required for half-accumulation ($t_{1/2}$) at DNA damage sites was 1.580 ± 0.150 s (Fig. 2, *b* and *c*). Quantitative fluorescence analysis indicates that the concentration of PARP1-GFP inside the laser path is nearly twice that of the nucleoplasm (Fig. 2*c*). These results confirm that PARP1 is not confined to a defined subnuclear structure but can migrate to sites of DNA breakage following exposure to DNA-damaging agents (25). The nuclear membranes of the microirradiated cells were intact, and cells remained viable during the experiment as defined by differential interference contrast images taken 2 min after the recorded time periods (Fig. 2*d*). Additionally, the presence of PARP1-GFP at sites of damage correlated with increased levels of PAR (Fig. 2*d*), which clearly reflects PARP enzymatic activity. Thus, from these data and the previously reported view that PARP1 is a DNA break sensor (12, 26), we conclude that PARP1 is one of the first molecules that is recruited to DNA breaks induced by laser microirradiation.

FRAP Measurements of Chromatin-bound and Free PARP1 after DNA Damage—To gain a better understanding of the interaction between PARP1 and DNA breaks, we applied FRAP analysis to measure the rate of PARP1-GFP exchange between the microirradiated region and the undamaged neighboring nucleoplasm (Fig. 3*a*). For quantitative analysis, fluorescence recovery in the bleached area, and intensities in nuclear regions as well as the background signal were quantified with minimal laser power. FRAP measurements revealed that the PARP1-GFP within the laser tracks had both reduced mobility and recovered up to 78% of the original relative level within 30 s (Fig. 3*b*). This indicates that a fraction of PARP1-GFP becomes transiently immobilized in microirradiated regions.

Dose-dependent Recruitment of PARP1 to Laser-generated DSB Sites—To determine the amount of PARP1-GFP recruited by the laser microirradiation, we directly analyzed the intensity of fluorescence accumulation at DNA damage sites by increasing the laser power. Increasing laser intensity, from 5% to 30%, led to an augmentation of PARP1 incorporation, which occurred over a broader distance across the laser trajectories (Fig. 4*a*), indicating that recruitment of PARP1 to localized DNA damage regions is highly dependent on the extent of DNA damage. The laser output set to 10% produced the sharpest redistribution of PARP1-GFP to DSB areas, whereas a decrease in energy yielded only partial recruitment, and increased laser power gave a dispersed pattern outside the laser path (Fig. 4*a*). For all experiments described in this study, we routinely employed low laser power level, which consistently produced detectable focused DSBs, as outlined by γ-H2AX staining (Fig. 4*b*) (15, 22). Quantitative measurements of fluorescent signals associated with the γ-H2AX antibody revealed that the amount

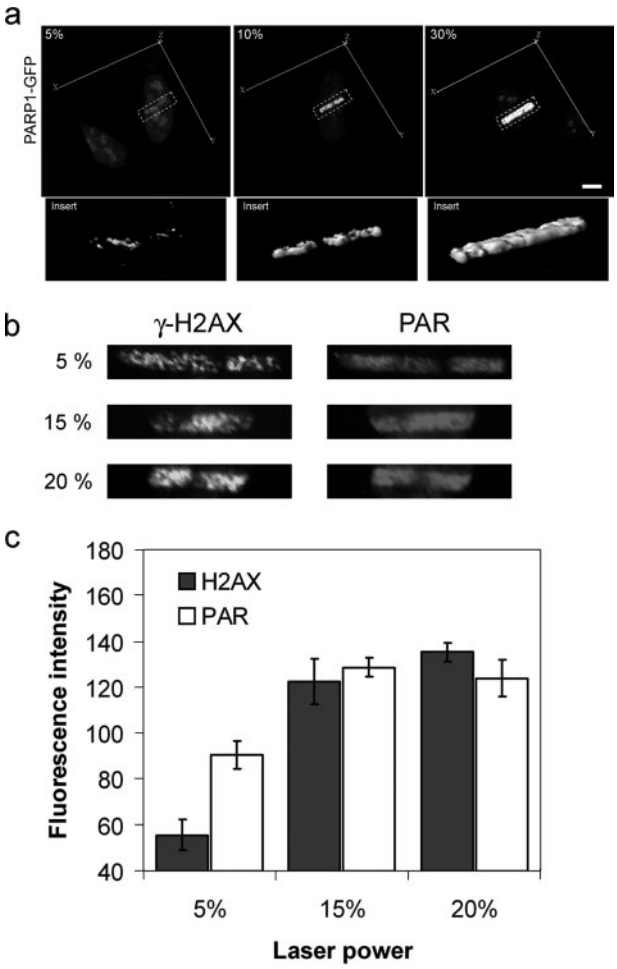

FIGURE 4. **Dose-dependent recruitment of PARP1 to locally induced DNA damage.** *a*, linear region across the entire nucleus were microirradiated with varying laser power. The energy output of the laser is indicated for each individual cell. *Bar*, 5 μm. The *insets* show three-dimensional images of the redistribution of PARP1-GFP in the microirradiated region. *b*, human cells were microirradiated with increasing laser power. The cells were fixed readily after induction of DSBs by laser microirradiation and processed for immunodetection of γ-H2AX and PAR synthesis. *c*, the *graph* summarizes quantification of fluorescence intensities associated to γ-H2AX and PAR as a function of laser power. Data are presented as mean ± S.E. from at least 20 cells for each treatment.

of DNA damage elicited by two-photon excitation of Hoechst 33258 in 5′-bromo-2′-deoxyuridine-sensitized cells is comparable with that generated by ionizing radiation in a dose range between 3 and 6 grays (Fig. 4*b*)[8] (2, 24). Together, these results indicate that there is a direct relation between the extent of γ-H2AX accumulation, the level of PAR synthesis, and the laser power level used to induce DSB (Fig. 4*c*).

PAR Synthesis and DSB-associated Protein Assembly at the DNA Damage Sites—We and others have recently observed that PAR forms foci that colocalize with γ-H2AX and phosphorylated ATM foci upon irradiation (13, 14, 27). Thus, to further define the spatial and temporal role of PAR synthesis in the early signaling of DNA damage formation, we analyzed cells that were fixed following multiphoton laser microirradiation in order to visualize endogenous PARP1 activation in human SK-

[8] J.-F. Haince, D. McDonald, A. Rodrigue, U. Déry, J.-Y. Masson, M. J. Hendzel, and G. G. Poirier, unpublished data.

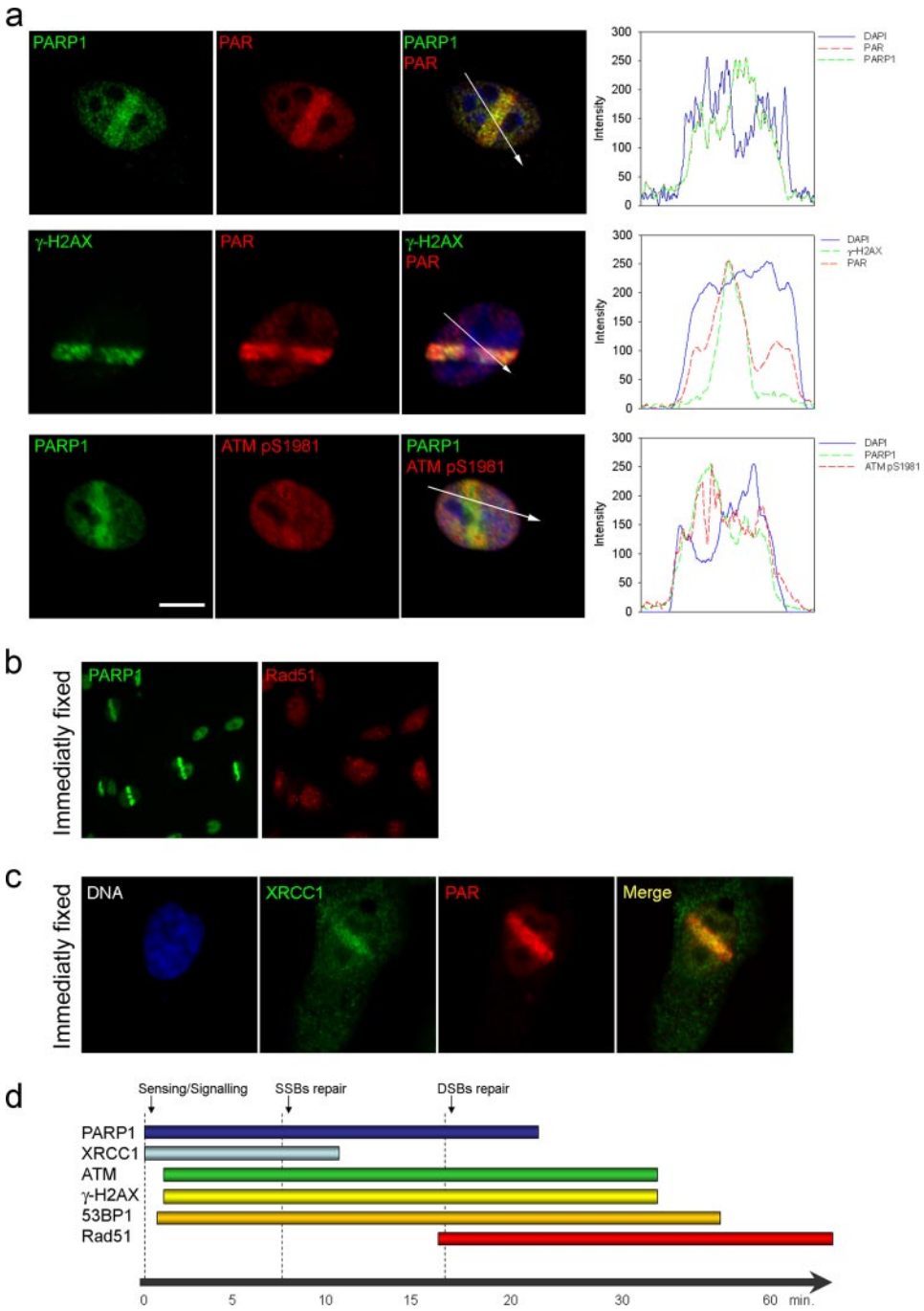

FIGURE 5. **Endogenous PARP1 colocalizes with the DSB-flanking proteins γ-H2AX and ATM following laser microirradiation.** *a*, human SK-N-SK cells were labeled for immunofluorescence immediately after laser microirradiation using anti-PARP1, anti-PAR, phospho-specific anti-H2AX S139, and phospho-specific anti-ATM S1981 antibody. Line profiles of background-corrected intensities were plotted for PARP1, PAR, γ-H2AX, ATM pS1981, and DAPI in each nucleus (*right*). The *arrows* indicate the direction of individual line scans from overlapping tracks in DAPI-stained nuclei. *Bar*, 10 μm. *b*, microirradiated cells were immediately fixed and labeled for immunofluorescence using anti-PARP1 and anti-Rad51 antibody. *c*, because laser microirradiation also generated SSBs, cells were labeled to visualize the SSB protein XRCC1 immediately after laser microirradiation. Synthesis of PAR was also labeled using anti-PAR antibody. Colocalization is shown in the *right panel*. DNA was stained with Hoechst 33258. *d*, schematic representation of temporal dynamics of SSB and DSB proteins recruitment to DNA damage induced by laser microirradiation.

N-SH cells (Fig. 5*a*). Immediately after microirradiation (less than 5 min), the cells were fixed with paraformaldehyde, and the localization and extent of DSB formation in a defined subnuclear region was studied by co-immunostaining for histone H2AX phosphorylation (γ-H2AX), activated ATM (phospho-serine 1981), and PARP1 and PAR synthesis. Immunofluorescence analysis established that endogenous PARP1 protein instantaneously concentrated within local "track" of DNA damage and was detectable for at least 30 min following the induction of the break (Fig. 5*a*). Poly(ADP-ribosyl)ation concentrated at DNA breaks immediately after laser microirradiation and persisted for at least an additional 15 min before it spread throughout the entire microirradiated nucleus (Fig. 5*a*). It has been previously reported that local irradiation by a proton microbeam induces instantaneous poly(ADP-ribosyl)ation, concomitant with the recruitment of ATM and Rad51 at sites of DNA damage (27). Examination of the DSB-induced phosphorylation of histone variant H2AX and ATM shows that PARP1 was efficiently recruited and activated in the same area as both DSB markers (Fig. 5*a*), whereas the immediate accumulation of the repair factor Rad51 following irradiation was not observed (Fig. 5*b*). It is not surprising that Rad51 is not readily observed in the microirradiated track, because accumulation of Rad51 protein requires the formation of single strand DNA at DNA damage site in order to be recruited, and it is necessary only for the later repair step (2).

Because laser microirradiation also generates SSBs, we tested whether or not XRCC1 protein is recruited to laser-induced DNA damage sites. As expected, XRCC1 is immediately recruited to DNA intermediates after laser microirradiation (Fig. 5*c*). Previous studies have revealed that XRCC1 accumulation in the microirradiated track was remarkably transient; most of the XRCC1 present at SSBs was lost after 10 min (28). The rapid kinetics of XRCC1 recruitment to and dissociation from DNA damage sites closely parallel the time needed to efficiently repair SSBs (28). In contrast, we found that although the initial recruitment of PARP1 was exceedingly rapid (Fig. 5*d*), PARP1 remained present in the laser track at its maximal concentration even 30 min after irradiation (Fig. 6*a*). This differs from XRCC1, which

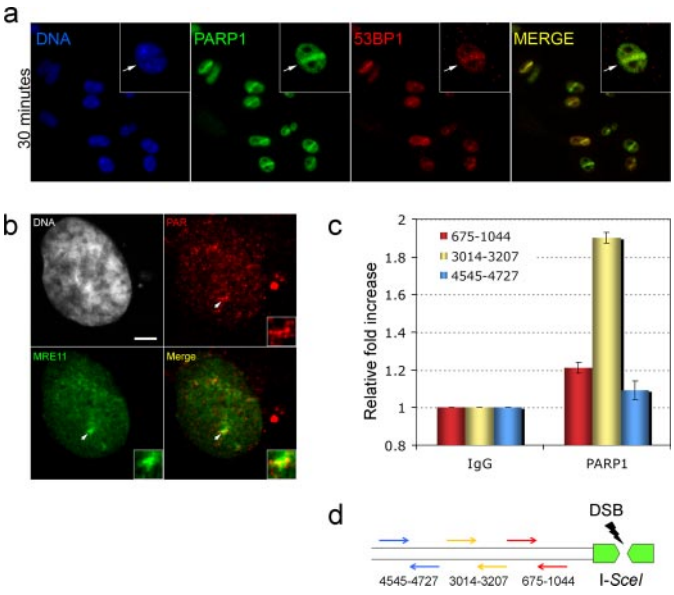

FIGURE 6. **PARP1 and DSB-interacting proteins co-localize at DNA damage sites.** SK-N-SH cells were fixed 30 min after laser microirradiation. *a*, endogenous PARP1 was colocalized with the DSB marker 53BP1. *Inset*, image of a single microirradiated cell. Nuclei were stained with DAPI. *b*, induction of a single DSB in SK-N-SH cells was performed through transfection of the I-*SceI* expression vector pCBASce, and immunofluorescence was conducted with antibodies against PAR and MRE11. *Inset*, PAR synthesis and MRE11 assembly at a unique DSB. *Bar*, 3 μm. *c*, the presence of endogenous PARP1 on a unique DSB was verified by ChIP analysis followed by real time PCR quantification at 675–1044, 3014–3207, and 4545–4727 nucleotides from the break (*red*, *yellow*, and *blue bars*, respectively). The *graph* represents the relative -fold increase of the PARP1 protein compared with an IgG control. The PCRs were performed in triplicate. *d*, schematic representation of the position of primers used for real time PCR quantification relative to the unique DSB created by I-*SceI in vivo*.

began to decline after 5 min (28). Consequently, PARP1 behavior is very reminiscent of that observed for proximal DSB regulators (2, 29, 30). In this way, PARP1 may organize the accumulation of DNA repair enzymes on multiple DNA lesions (Fig. 5*d*). This conclusion was further confirmed by the colocalization with 53BP1 observed at DNA damage sites 30 min after irradiation (Fig. 6*a*). These observations are consistent with the idea that DSB repair pathways might benefit from the increased local concentration of PARP1 observed at DNA damage sites generated by irradiation.

PARP1 Localizes to a Unique DSB Site in Vivo—To determine whether a DSB is a type of DNA lesion that triggers the recruitment and retention of PARP1 at DNA damage sites, we created a unique DSB in SK-N-SH cells using the I-*SceI* repair system (20). Following I-*SceI* cleavage, we observed the formation of a single focus of MRE11 (Fig. 6*b*). PARP1-dependent PAR synthesis is simultaneously detected at this focal point (Fig. 6*b*), suggesting that PAR might be a signal for the recruitment of DNA damage proteins on a unique site-specific DSB. In order to increase the level of resolution of the light microscopy, we designed oligonucleotides to perform ChIP analysis on a unique site-specific DSB created by I-*SceI* (20). ChIP analysis performed 6 h after transfection of an I-*SceI*-encoded vector revealed an enrichment in PARP1 (~2-fold) at 3014–3207 bp from the break (Fig. 6, *c* and *d*). Although it is not possible to exclude low level (~1.2-fold enrichment) or transient binding of PARP1 close to the site-specific DSB generated by I-*SceI* in this assay, our results demonstrated that PARP1 was efficiently recruited in adjacent regions of the DSB (Fig. 6*c*). Similar observations have been made concerning the distribution of other DSB sensors, such as ATM and its target H2AX (29). Thus, our results identified clear parallels between PARP1 distribution around a site-specific DSB and distribution of both ATM and phosphorylated H2AX in a broad region flanking the DSB site (29). In contrast to DSB sensors, the distribution of most repair proteins has been observed directly at DSB sites (20, 29).

PARP1 Is Required for Rapid Recruitment of MRE11 and NBS1 at DSB Sites—Because the selective recruitment of a specialized DNA damage sensor might be required to enhance the efficiency of different DNA repair pathways, we extended our analysis to the recruitment kinetics of the MRN complex. The components of the MRN complex are key DSB sensors associated with chromatin after laser microirradiation (2). Importantly, the assembly and transient immobilization of the MRN complex required the presence of Mdc1 at DSB sites (30). Our time lapse microscopy of fluorescently tagged proteins reveals that PARP1 is the first protein to accumulate at microirradiated sites (Fig. 5*d*), preceding even Mdc1 accumulation (30). This observation prompted us to determine whether or not PARP1 modulates the kinetics and amplitude of MRN complex assembly after laser microirradiation. First, we analyzed the kinetics of assembly for the MRN complex proteins MRE11 and NBS1 at laser-induced DSB in wild-type cells. To ensure identical experimental conditions, we transiently expressed YFP-MRE11 or GFP-NBS1 in PARP1-proficient cells and imaged cells with nearly physiological expression of fluorescently tagged proteins (Fig. 7*a*). The detailed mathematical analysis of YFP-MRE11-associated fluorescence demonstrated that $t_{1/2}$ was ~13.102 s ± 0.559 s (Fig. 7*c*), which is 10 times slower than what we observed for PARP1-GFP (Fig. 2*d*). Likewise, cytologically discernable foci of GFP-NBS1 were only observed after 10 s and reached steady-state equilibrium between 1 and 2 min after microirradiation (Fig. 7, *a* and *d*). The $t_{1/2}$ for GFP-NBS1 recruitment is 28.193 ± 1.395 s, which is consistent with earlier reports (23, 30).

Next, we measured the increase of the fluorescence associated with both YFP-MRE11 and GFP-NBS1 at the DSB sites in cells genetically deficient for PARP1 protein. Strikingly, live cell fluorescence analysis showed that YFP-MRE11 does not appear to be recruited at a significant level in PARP1-deficient cells (Fig. 7*b*), and the amount of YFP-MRE11 at saturation was significantly reduced relative to that observed in PARP1-proficient cells (Fig. 7*c*). The redistribution of GFP-NBS1 in the microirradiated track is also significantly altered in PARP1-deficient cells (Fig. 7*b*). After 60 s, the amount of GFP-NBS1 recruited at DSB sites is only one-third of that observed in normal cells (Fig. 7*d*). Collectively, these *in vivo* measurements identify PARP1 as a key upstream determinant for the assembly of the MRN complex at defined regions of DSBs. This observation further supports the notion that PARP1 is a processing factor involved in the spatial redistribution of protein in the DSB-flanking regions following DNA damage.

PARP1 Physically Interacts with MRE11—In order to determine whether or not MRE11 interacts with PARP1 and/or PAR, immunoprecipitation (IP) of PARP1 was conducted in human cells subjected or not to etoposide treatment (1 h, 50 μM). IP experiments using anti-PARP1 antibody in human cells

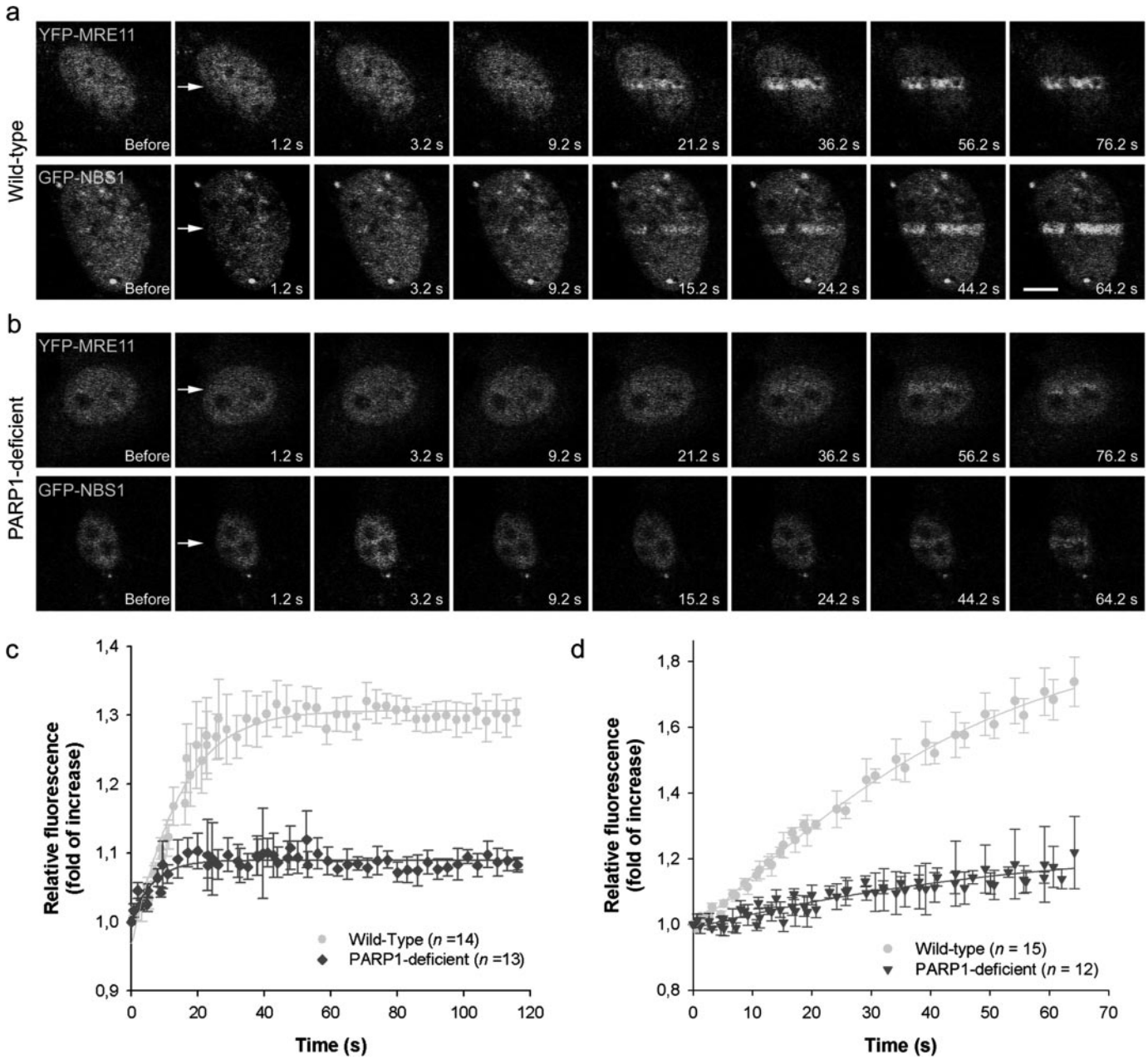

FIGURE 7. **Rapid accumulation of MRE11 and NBS1 at DSB sites requires the nuclear enzyme PARP1.** *a*, live cell imaging of wild-type cells (C3H10T$_{1/2}$) expressing either YFP-MRE11 or GFP-NBS1. After microirradiation, YFP-MRE11 and GFP-NBS1 rapidly accumulate at sites of DNA damage. *Bar*, 5 μm. *b*, live cell imaging of fluorescently tagged MRE11 and NBS1 proteins after laser-generated DSB in PARP1-deficient cells (A1) shows differences in recruitment of YFP-MRE11 and GFP-NBS1 to DSB sites compared with wild-type cells show in *a*. Confocal images were captured at 500-ms intervals for 120 s after microirradiation. The *arrows* indicate nuclear regions containing laser-induced DSB. Fluorescently tagged proteins and times elapsed after microirradiation are indicated. *c*, the kinetics of MRE11 association with DSB from both wild-type and PARP1-deficient cells were plotted. *d*, *graph* reviews the real time measurements of NBS1 accumulation at DSB sites from both wild-type and PARP1-deficient cells. Quantitative measurements of YFP-MRE11 and GFP-NBS1 accumulation in regions of laser-induced DSB represent the average fluorescence ± S.E. from more than 10 individual cells.

revealed that PARP1 interacts with MRE11 (Fig. 8*a*). In addition, the DNA damage proteins NBS1 and SMC1 were pulled down when PARP1 was immunoprecipitated (Fig. 8*a*). IP of endogenous MRE11 in SK-N-SH cells was also conducted to verify the specificity of the interaction with PARP1. As expected, PARP1 was found in the MRE11 IP along with the DSB-associated proteins NBS1 and SMC1 (Fig. 8*b*).

Nuclear Retention of MRE11 Is Impaired in PARP1-deficient Cells—Because PARP1 is required for the rapid accumulation of MRE11 and NBS1 at DSB sites, the specific interaction between PARP1 and MRE11 might play a role in recruitment of both MRE11 and NBS1 at DSB. This phenomenon is probably due to the fact that poly(ADP-ribosyl)ation promotes chromatin relaxation in the vicinity of the DSB (5) and facilitates the spatial redistribution of protein in the DSB-flanking regions. To rigorously test this hypothesis, we performed cellular fractionation using successive detergent extraction (19). It has been shown previously that following exposure to DNA-damaging agents, a proportion of DSB-associated proteins becomes resistant to detergent extraction and is probably retained at

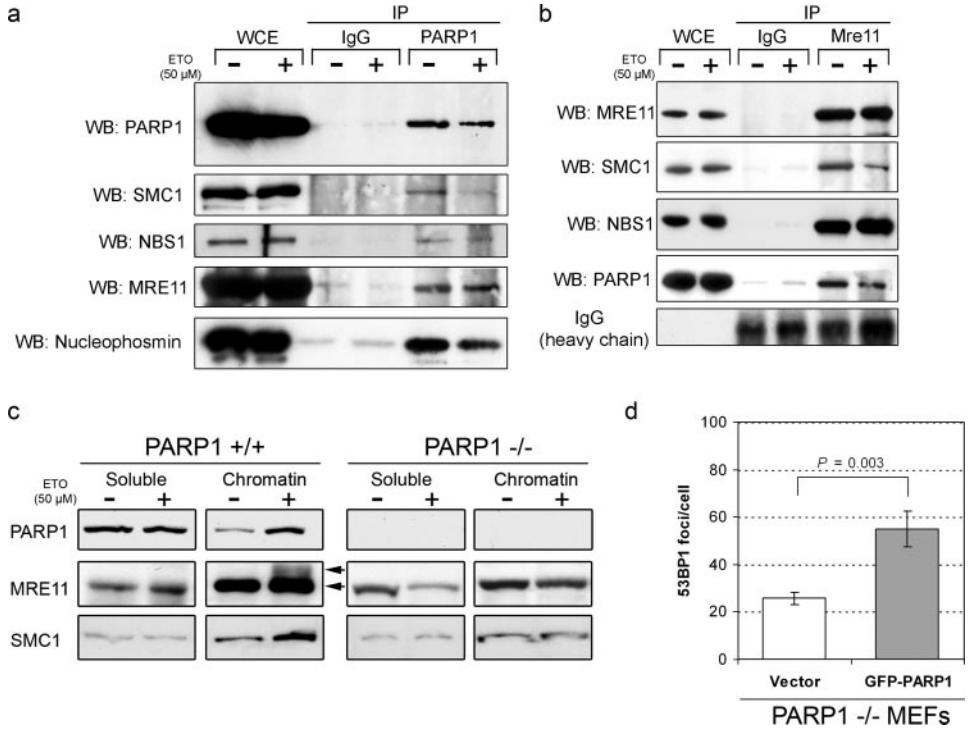

FIGURE 8. **Endogenous PARP1 interacts with MRE11 at DSB sites.** Shown is *in vivo* IP analysis of PARP1 (*a*) and MRE11 protein (*b*) using SK-N-SH whole cell extracts (*WCE*) treated or not with etoposide (50 μM, 1 h). *c*, wild-type MEF cells (*left*) or PARP1-deficient cells (*right*) were treated or not with 50 μM etoposide. One hour later, cells were fractionated with successive detergent extraction, and extracts were immunoblotted as indicated. *d*, quantification of DNA damage-induced 53BP1 foci per cell in PARP1-deficient cells transfected or not with a GFP-PARP1 vector. *Error bars*, S.E. *WB*, Western blot.

DSB sites (3, 4). In PARP1$^{+/+}$ cells treated with etoposide (50 μM, 1 h), the amounts of DSB-flanking proteins MRE11 and SMC1 were higher in the extraction-resistant chromatin fraction (Fig. 8*c*). Notably, we consistently observed a slower migrating band of MRE11 in chromatin fraction (Fig. 8*c*), which is supportive of a phosphorylation of MRE11 following exposure to DNA-damaging agent (31). Correlating with the retention of MRE11 in the chromatin fraction, we found that PARP1 also accumulated in the extraction-resistant fraction after etoposide treatment (Fig. 8*c*). In contrast, examination of biochemical fractions from PARP1-deficient cells revealed that neither the accumulation nor the slower migrating form of MRE11 could be detected in the chromatin fraction of etoposide-treated cells. Additionally, no detectable change in the chromatin was observed for SMC1 between treated and untreated PARP1-deficient cells.

In order to understand the meaning of this interaction at DNA damage level, we evaluated the DNA damage response in PARP1-deficient cells and in cells expressing a functional PARP1-GFP fusion protein. It is already known that PARP1-deficient cells form a reduced number of DNA damage protein foci (Fig. 8*d*) (13, 14). Here we show that expression of PARP1-GFP in PARP1-deficient cells restores the cellular response to DSBs (Fig. 8*d*). Quantitative immunofluorescence analysis of etoposide-induced DNA damage revealed that the number of 53BP1 foci per cell is significantly higher ($p = 0.003$) in PARP1-deficient cells transfected with the PARP1-GFP vector, which allows expression of an active PARP1. Taken together, the work presented here documents for the first time that, following DNA damage induction, PARP1 interacts with MRE11 and assists in the recruitment of MRE11 to the so-called DNA repair foci (Fig. 8, *a–d*).

MRE11 Has a Putative PAR-binding Domain—Based on the biochemical properties of PAR, it is reasonable to envisage that poly(ADP-ribosyl)ation plays a role in attracting the MRN complex to sites of DNA damage. We found that in response to etoposide treatment, local PAR synthesis is accompanied by MRE11 foci formation in the close vicinity of damaged DNA (Fig. 9*a*). Quantitative image analysis also established that 42.1% of MRE11 foci efficiently colocalize with sites of PAR synthesis (Fig. 9*a*), indicating that PAR molecules might mediate a signal emerging from DSB sites that is necessary for the proper redistribution of repair proteins to damaged chromatin regions. Although MRE11 interacts directly with PARP1, there is increasing evidence that many DNA damage response proteins have a functional PAR-binding domain (32, 33). The typical PAR-binding motif comprises ~20 amino acids and is characterized by the presence of hydrophobic amino acids (H; ACGVILMFYW) spaced by basic amino acids (B; HKR) and by an accumulation of basic residues (KR) at the N-terminal site of the motif. Accordingly, we have identified the presence of a putative PAR-binding motif in human MRE11 by amino acid sequence similarity with the PAR-binding consensus sequence, suggesting that the interaction with PARP might occur via PAR. The PAR-binding motif of MRE11 has been identified at positions 559–591 (Fig. 9*b*). Using a nitrocellulose-PAR binding assay, we found that purified MRE11 bound both PAR and poly(ADP-ribosyl)ated PARP1 (Fig. 9*c*). To determine whether or not this specific motif is required for MRE11-PAR interaction, we replaced the important arginine residues with alanine in the MRE11 R/A mutant. As expected, purified MRE11 protein mutated in the PAR-binding region did not bind to PAR (Fig. 9*c*). In addition, it was recently demonstrated that ATM interacts with PAR (13), which stimulated the ATM kinase activity *in vitro* (34) and *in vivo* (14). Because MRE11 also interacted with PAR (Fig. 9*c*), we investigated whether PAR has a direct effect on MRE11 exonuclease activity. Purified MRE11 (2 nM) was incubated with a fixed concentration (100 nM) of a 63-bp double-stranded DNA substrate and an increasing amount of PAR (0.002–2 μM) (Fig. 9*d*). Surprisingly, we found that a 20-fold excess of PAR compared with double-stranded DNA substrate prevented the MRE11 nuclease activity (Fig. 9*d*). At this high concentration of PAR, the inhibition of MRE11 nuclease activity observed in this *in vitro* assay was probably due to the fact that MRE11 will bind

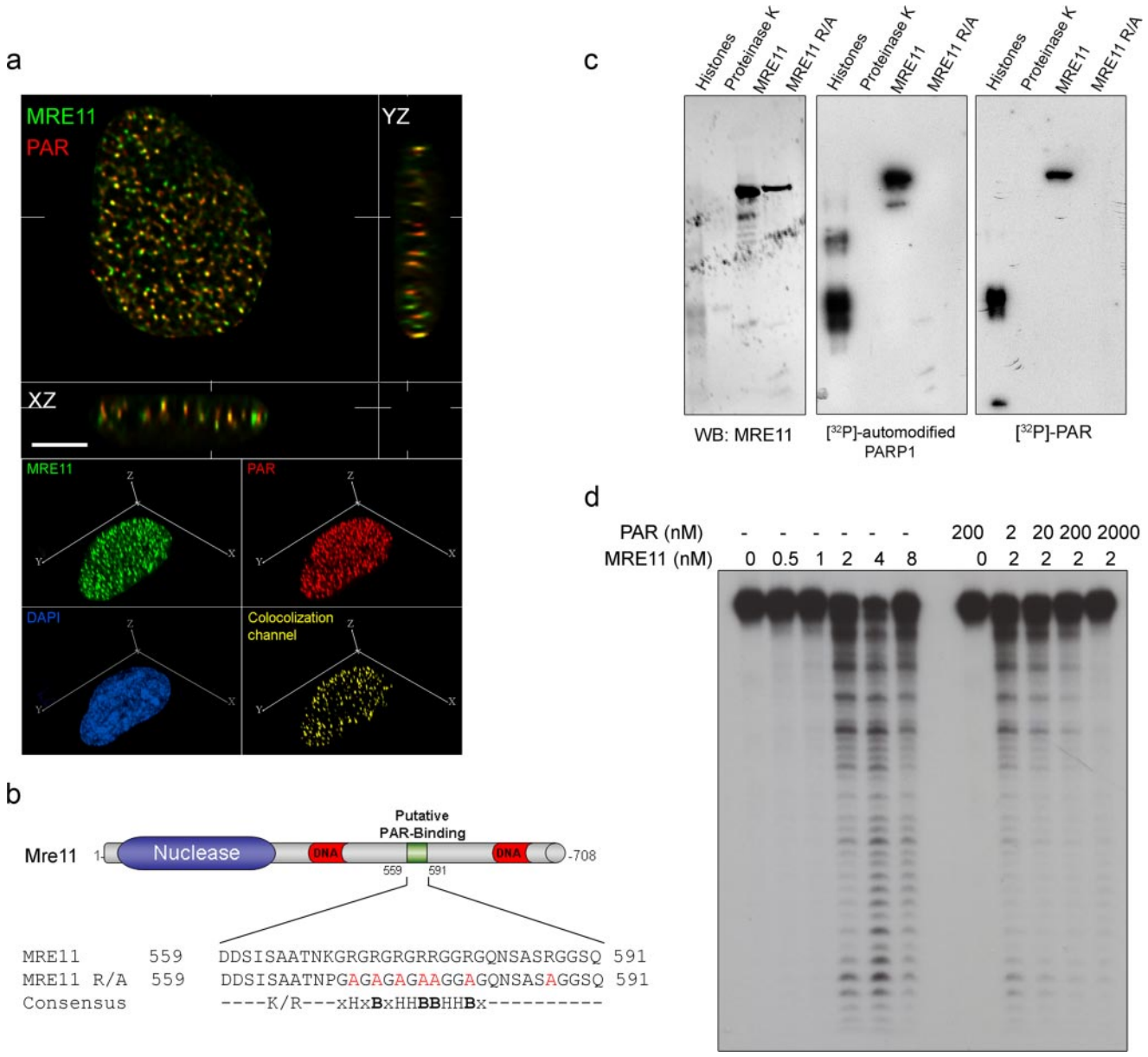

FIGURE 9. **MRE11 binds poly(ADP-ribose).** *a*, human cells were exposed for 1 h to 50 μM etoposide and then immunostained with anti-PAR polyclonal antibody 96-10 and anti-MRE11 monoclonal antibody. Colocalization of MRE11 foci with sites of PAR synthesis is shown. Images were collected as *z*-series, and only a single representative deconvolved plane is presented. *Scale bars*, 3 μm. The *four bottom panels* show three-dimensional renderings of MRE11, PAR, DNA (counterstained with DAPI), and the colocalization channel. *b*, putative PAR-binding motif on MRE11 proteins. *c*, purified MRE11 binds specifically to automodified PARP1 and PAR *in vitro*, whereas MRE11 R/A mutant failed to bind both. *First panel*, Western blot of purified wild-type and mutant MRE11 proteins. *d*, MRE11 exonuclease assays were performed on a ^{32}P-5′-end-labeled 63-bp double-stranded DNA substrate with the indicated amounts of MRE11 and PAR.

to PAR molecules instead of binding to its double-stranded DNA substrate. These results support the hypothesis that PAR or poly(ADP-ribosyl)ated PARP1 serves a function in the recruitment of proteins at DNA lesions.

DISCUSSION

In the present study, we performed a detailed spatiotemporal analysis of PARP1 recruitment to DSBs. We first investigated the accumulation of fluorescently tagged PARP1 to defined sites of DNA damage introduced by multiphoton laser microirradiation *in vivo* using a PARP1-deficient cell line expressing biologically active GFP-tagged PARP1. An important observation presented here is that PARP1 accumulation at photoinduced DSBs can be detected as early as 500 ms postirradiation and is maximal by 5 s. The remarkable kinetics of PARP1 within localized DSB regions further corroborated the conclusion that PARP1 is rapidly recruited to and transiently associates with DSBs. FRAP analysis also reveals that a large proportion of PARP1 remained mobile and can rapidly exchange with the pool of PARP1 located in undamaged nucleoplasm. The observation that PARP1 is only transiently maintained to DNA damage sites suggests that laser-induced microirradiation generates a particular type of lesion to which PARP1 binds. To validate that a DSB is a type of DNA lesion that triggers PARP1 activation, we generated a single site-specific DSB using the I-*SceI* endonuclease. Transient expression of I-*SceI* in human cells

resulted in a measurable activation of PARP1, which has been detected by PAR synthesis and binding of MRE11 to the site-specific DSB. ChIP analysis using a specific PARP1 antibody confirmed the presence of PARP1 in the vicinity of the I-*SceI*-induced DSB. Interestingly, the distribution of the damage response kinase ATM and its major target H2AX around a site-specific DSB are both about 3 kb of the break (29). The presence of both enzymes at 3 kb is consistent with our new findings, which illustrates that PARP1 facilitates, by polymer formation, a rapid change in chromatin structure that facilitates access of the MRN complex to the break. As we recently showed in a previous paper (13), ATM is positively modulated by PAR, and together these data suggest a dynamic series of molecular events that modulate chromatin structure and provide an explanation for the accumulation of PARP1 about 3 kb from the break.

Most importantly, we found that PARP1 seems to be required for rapid accumulation of MRE11 protein at DSBs. This is further supported by the fact that despite a progressive accumulation of the NBS1 protein at DSB sites in wild-type cells, only a faint fluorescent signal associated with GFP-NBS1 was detected in PARP1-deficient cells. Interestingly, MRE11 was specifically detected in PARP1 immunoprecipitates, suggesting that PARP1 and MRE11 are indeed found in a common complex. In mammalian cells, the presence of PARP1 and MRE11 proteins in a functional complex has been described as an important mechanism in resolving recombination-induced DNA lesions (35). Similarly, PARP1 is known to be an important component of the DNA damage response in *Caenorhabditis elegans*, where it has been found to interact with MRE11 (36). In addition to the direct interaction between PARP1 and MRE11, we have identified a putative PAR-binding domain in MRE11, suggesting that the recruitment of MRN complex at DSBs might occur through interactions with PAR molecules.

This study has revealed a number of critical points with respect to the spatial and temporal aspects of the reorganization that takes place following DNA damage introduction in living mammalian cells. Our data provide the first *in vivo* evidence that PARP1 is required for the proper dynamic assembly of DSB sensors and the recruitment of key components of the early ATM-dependent signaling pathway. This provides new insight into the dynamic nature of protein interaction networks in the nuclei of living cells. Based upon our results, we would predict that once activated, PARP1 automodification rapidly triggers its dissociation from the DNA template and opens the chromatin structure to give access to repair proteins. As a direct result, the time needed for MRE11 and NBS1 to accumulate within the DSB-flanking chromatin is significantly increased in cells lacking PARP1. Together, these results imply that defects observed in PARP1 null MEFs could be explained by an impaired function of the MRN complex. Several lines of evidence indicate that PARP1 null mouse cells share cellular phenotypes observed when the MRN complex is compromised, although the clinical phenotypes may not overlap significantly (37, 38). Clearly, both PARP1 and MRN-deficient cells exhibit ionizing radiation sensitivity, chromosomal aberrations, increased sister chromatin exchange, and reduced DNA repair. Interestingly, two recent papers have shown that PARP1-deficient cells have reduced HR repair and increased NHEJ (7, 8), suggesting that PARP1 regulates the balance between HR and NHEJ. The dynamic assembly and PAR-binding properties of MRE11 revealed in this study support a model in which PAR, via interaction with the MRN complex, plays an early role as a sensory molecule of the DNA damage response.

Because the kinetics reported here are essentially in agreement with previous findings (2, 15, 16, 30), we could not exclude the possibility that the assembly of repair complex through PAR-binding interaction is not the only way to target those complexes to DNA breaks. Indeed, the accumulation of PARP1 at DSB enhances, but is not absolutely required for, the DSB signaling pathway and later repair processes, such as HR and NHEJ (13). Additionally, *in vitro* experiments with purified proteins have shown that MRE11 can bind DNA breaks and recruit ATM without PARP1 (39). It is important to note, however, that these *in vitro* studies were done on naked DNA templates rather than native folded chromatin structures.

In conclusion, the unique methodology used in this study has enabled us to directly demonstrate that PARP1 efficiently accumulates close to a site-specific DSB, where it markedly modulated the recruitment of MRN complex to DNA damage sites. This is consistent with the fact that poly(ADP-ribosyl)ation may function to organize recruitment of DSB repair proteins to the DNA strand break by noncovalent PAR-binding interaction. Our data uncover an emerging role of PARP1 as a regulator of genome maintenance pathways. These results help to reconcile the current discrepancies concerning the direct participation of PARP1 in DSB sensing and signaling pathways.

Acknowledgments—We thank S. Richard for kindly providing the fluorescently tagged MRE11 proteins. We are also grateful to Isabelle Brodeur for the development of the I-SceI repair system in SK-N-SK cells and for ChIP analysis.

REFERENCES

1. O'Driscoll, M., and Jeggo, P. A. (2006) *Nat. Rev. Genet.* **7,** 45–54
2. Bekker-Jensen, S., Lukas, C., Kitagawa, R., Melander, F., Kastan, M. B., Bartek, J., and Lukas, J. (2006) *J. Cell Biol.* **173,** 195–206
3. Carson, C. T., Schwartz, R. A., Stracker, T. H., Lilley, C. E., Lee, D. V., and Weitzman, M. D. (2003) *EMBO J.* **22,** 6610–6620
4. Uziel, T., Lerenthal, Y., Moyal, L., Andegeko, Y., Mittelman, L., and Shiloh, Y. (2003) *EMBO J.* **22,** 5612–5621
5. Kim, M. Y., Zhang, T., and Kraus, W. L. (2005) *Genes Dev.* **19,** 1951–1967
6. Schreiber, V., Dantzer, F., Ame, J. C., and de Murcia, G. (2006) *Nat. Rev. Mol. Cell. Biol.* **7,** 517–528
7. Wang, M., Wu, W., Wu, W., Rosidi, B., Zhang, L., Wang, H., and Iliakis, G. (2006) *Nucleic Acids Res.* **34,** 6170–6182
8. Hochegger, H., Dejsuphong, D., Fukushima, T., Morrison, C., Sonoda, E., Schreiber, V., Zhao, G. Y., Saberi, A., Masutani, M., Adachi, N., Koyama, H., de Murcia, G., and Takeda, S. (2006) *EMBO J.* **25,** 1305–1314
9. McCabe, N., Turner, N. C., Lord, C. J., Kluzek, K., Bialkowska, A., Swift, S., Giavara, S., O'Connor, M. J., Tutt, A. N., Zdzienicka, M. Z., Smith, G. C. M., and Ashworth, A. (2006) *Cancer Res.* **66,** 8109–8115
10. Farmer, H., McCabe, N., Lord, C. J., Tutt, A. N., Johnson, D. A., Richardson, T. B., Santarosa, M., Dillon, K. J., Hickson, I., Knights, C., Martin, N. M., Jackson, S. P., Smith, G. C., and Ashworth, A. (2005) *Nature* **434,** 917–921
11. Bryant, H. E., Schultz, N., Thomas, H. D., Parker, K. M., Flower, D., Lopez, E., Kyle, S., Meuth, M., Curtin, N. J., and Helleday, T. (2005) *Nature* **434,** 913–917

12. Lindahl, T., Satoh, M. S., Poirier, G. G., and Klungland, A. (1995) *Trends Biochem. Sci.* **20,** 405–411
13. Haince, J.-F., Kozlov, S., Dawson, V. L., Dawson, T. M., Hendzel, M. J., Lavin, M. F., and Poirier, G. G. (2007) *J. Biol. Chem.* **282,** 16441–16453
14. Aguilar-Quesada, R., Munoz-Gamez, J. A., Martin-Oliva, D., Peralta, A., Valenzuela, M. T., Matinez-Romero, R., Quiles-Perez, R., Menissier-de Murcia, J., de Murcia, G., de Almodovar, M. R., and Oliver, F. J. (2007) *BMC Mol. Biol.* **8,** 29
15. Kruhlak, M. J., Celeste, A., Dellaire, G., Fernandez-Capetillo, O., Muller, W. G., McNally, J. G., Bazett-Jones, D. P., and Nussenzweig, A. (2006) *J. Cell Biol.* **172,** 823–834
16. Bradshaw, P. S., Stavropoulos, D. J., and Meyn, M. S. (2005) *Nat. Genet.* **37,** 193–197
17. Lever, M. A., Th'ng, J. P., Sun, X., and Hendzel, M. J. (2000) *Nature* **408,** 873–876
18. McDonald, D., Carrero, G., Andrin, C., de Vries, G., and Hendzel, M. J. (2006) *J. Cell Biol.* **172,** 541–552
19. Andegeko, Y., Moyal, L., Mittelman, L., Tsarfaty, I., Shiloh, Y., and Rotman, G. (2001) *J. Biol. Chem.* **276,** 38224–38230
20. Rodrigue, A., Lafrance, M., Gauthier, M. C., McDonald, D., Hendzel, M., West, S. C., Jasin, M., and Masson, J. Y. (2006) *EMBO J.* **25,** 222–231
21. Boisvert, F. M., Dery, U., Masson, J. Y., and Richard, S. (2005) *Genes Dev.* **19,** 671–676
22. Meldrum, R. A., Botchway, S. W., Wharton, C. W., and Hirst, G. J. (2003) *EMBO Rep.* **4,** 1144–1149
23. Lukas, C., Falck, J., Bartkova, J., Bartek, J., and Lukas, J. (2003) *Nat. Cell Biol.* **5,** 255–260
24. Mari, P. O., Florea, B. I., Persengiev, S. P., Verkaik, N. S., Bruggenwirth, H. T., Modesti, M., Giglia-Mari, G., Bezstarosti, K., Demmers, J. A., Luider, T. M., Houtsmuller, A. B., and van Gent, D. C. (2006) *Proc. Natl. Acad. Sci. U. S. A.* **103,** 18597–18602
25. Yung, T. M., Sato, S., and Satoh, M. S. (2004) *J. Biol. Chem.* **279,** 39686–39696
26. Kim, J. S., Krasieva, T. B., Kurumizaka, H., Chen, D. J., Taylor, A. M., and Yokomori, K. (2005) *J. Cell Biol.* **170,** 341–347
27. Tartier, L., Spenlehauer, C., Newman, H. C., Folkard, M., Prise, K. M., Michael, B. D., Menissier-de Murcia, J., and de Murcia, G. (2003) *Mutagenesis* **18,** 411–416
28. Mortusewicz, O., Rothbauer, U., Cardoso, M. C., and Leonhardt, H. (2006) *Nucleic Acids Res.* **34,** 3523–3532
29. Berkovich, E., Monnat, R. J., Jr., and Kastan, M. B. (2007) *Nat. Cell Biol.* **9,** 683–690
30. Lukas, C., Melander, F., Stucki, M., Falck, J., Bekker-Jensen, S., Goldberg, M., Lerenthal, Y., Jackson, S. P., Bartek, J., and Lukas, J. (2004) *EMBO J.* **23,** 2674–2683
31. Dong, Z., Zhong, Q., and Chen, P.-L. (1999) *J. Biol. Chem.* **274,** 19513–19516
32. Malanga, M., and Althaus, F. R. (2005) *Biochem. Cell Biol.* **83,** 354–364
33. Pleschke, J. M., Kleczkowska, H. E., Strohm, M., and Althaus, F. R. (2000) *J. Biol. Chem.* **275,** 40974–40980
34. Goodarzi, A. A., and Lees-Miller, S. P. (2004) *DNA Repair* **3,** 753–767
35. Brown, M. L., Franco, D., Burkle, A., and Chang, Y. (2002) *Proc. Natl. Acad. Sci. U. S. A.* **99,** 4532–4537
36. Boulton, S. J., Gartner, A., Reboul, J., Vaglio, P., Dyson, N., Hill, D. E., and Vidal, M. (2002) *Science* **295,** 127–131
37. Huber, A., Bai, P., Menissier-de Murcia, J., and de Murcia, G. (2004) *DNA Repair* **3,** 1103–1108
38. Kang, J., Bronson, R. T., and Xu, Y. (2002) *EMBO J.* **21,** 1447–1455
39. Lee, J. H., and Paull, T. T. (2004) *Science* **304,** 93–96